Radiation and Scattering from Infinite Periodic Printed Antennas with Inhomogeneous Media

Wen-Jiunn Tsay and David M. Pozar, *Fellow, IEEE*

***Abstract*— The hybrid method of moments (MoM)/Green's function method [1] technique is applied to infinite periodic printed antenna arrays containing dielectric inhomogeneities. The solution uses an integral equation for an infinite periodic printed array on or over a homogeneous dielectric substrate [2], coupled with equivalent volume polarization currents for dielectric inhomogeneities on top of the homogeneous substrate. Volume pulse-basis functions were used to expand the volume polarization currents. A hybrid MoM/Green's function method solution was then obtained through the matrix form of the problem. The two-dimensional (2-D) solution of plane wave scattering from a grounded dielectric slab was used to validate the reaction impedance of the dielectric inhomogeneity. Several infinite periodic printed dipole arrays with dielectric supports and overlays were studied with this solution and good agreement was observed between the hybrid MoM/Green's function method and waveguide simulator experiments.**

***Index Terms*—Microstrip antennas, nonhomogeneous media.**

I. Introduction

THE objective of this work is to develop a hybrid method of moments (MoM)/Green's function solution (abbreviated as the hybrid moment method) to analyze three-dimensional (3-D) periodic antenna and scattering problems involving a dielectric substrate with dielectric inhomogeneities. There are four types of geometries in which we are interested. Fig. 1(a) shows an infinite planar array of printed antennas on a homogeneous grounded dielectric substrate; Fig. 1(b) shows an infinite planar array of printed antennas with dielectric barriers; Fig. 1(c) shows an infinite planar array of printed antennas with dielectric supports; and Fig. 1(d) shows an infinite planar array of printed antennas with dielectric overlays. By analysis of these geometries, we can study the effect of dielectric inhomogeneities on the performance of an infinite periodic array antenna where potentially improved bandwidth or scan range may be achieved and novel antenna geometries may be investigated.

One application of such geometries is to obtain an additional degree of freedom for an array beyond the substrate thickness to optimize the impedance bandwidth and scanning range of large printed arrays. Pozar and Schaubert [2] discovered that surface wave coupling can lead to scan blindness where no effective power is transmitted or received by the array.

Manuscript received August 17, 1995; revised August 22, 1996.

W.-J. Tsay is with Anritsu/Wiltron Company, Morgan Hill, CA 95037 USA.
D. M. Pozar is with the Department of Electrical and Computer Engineering, University of Massachusetts at Amherst, Amherst, MA 01003 USA.

Publisher Item Identifier S 0018-926X(98)08883-8.

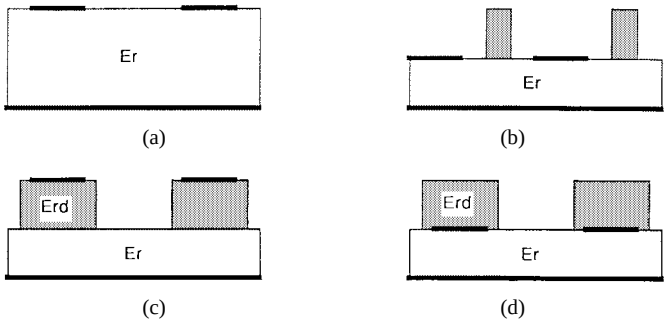

Fig. 1. Printed antenna arrays with (a) homogeneous substrate, (b) dielectric barriers, (c) dielectric supports, and (d) dielectric overlays.

Through the interruption of surface waves or other propagating modes that cause scan blindness, it may be possible to control blindness by using inhomogeneous loading [3], [4] and still maintain a reasonable impedance bandwidth.

Another application is to increase the bandwidth of an array by using dielectric overlays. Generally speaking, any improvement in bandwidth for printed antennas can only be achieved by an increase in volume or a loss in efficiency [5]. Hall *et al.* [6] have experimentally shown that the bandwidth of alumina patches can be increased by a factor of 16 by overlaying pieces of substrate. Such a dielectric overlay can be considered as a type of resonator antenna, as reported by McAllister *et al.* [7]. Recently, Kishk *et al.* [8] have studied the problem of a dielectric disk antenna above a grounded dielectric substrate. By replacing the conducting patch with a low-loss dielectric disk resonator, they were able to achieve 30% bandwidth. These examples suggest that if the configuration in Fig. 1(d) can be implemented, it may be possible to significantly increase the bandwidth of a large array.

All of the above configurations can be categorized as problems of radiation and scattering in periodic inhomogeneous media. If a solution for these problems is available, we will be able to solve a large variety of useful radiation and scattering problems involving inhomogeneous media.

The finite-difference time-domain (FDTD) method is a useful computational technique for a wide variety of problems in radiation and scattering, especially when inhomogeneous material are involved [9]–[11]. However, the FDTD method to date has proved to be difficult to apply to problems of this type [12]–[16]. While many problems have been treated via the moment method and other full-wave solutions [2], [17], these techniques are generally limited to geometries without

transverse material inhomogeneities. Hybrid moment-method solutions have been implemented to solve inhomogeneous problems for a single antenna [1], [18]. This paper extends this concept to an infinite planar array with dielectric inhomogeneities. A disadvantage of this method is that the derivation of the dyadic Green's function and the integral equation matrix elements are tedious and complicated. Also, memory requirements and central processing unit (CPU) time increase sharply as the electrical size of a unit cell in the array becomes large.

Following the standard moment-method procedure for an infinite periodic array antenna [2], the equivalent volume polarization current that is induced inside a dielectric inhomogeneity is used to create a second integral equation according to the volume equivalence theorem. To independently verify the reaction impedance elements generated by the dielectric inhomogeneity, two-dimensional (2-D) scattering from a grounded dielectric slab with parallel polarization plane wave incidence was studied. Volume pulse-basis functions were chosen to expand the equivalent polarization current. Excellent agreement is observed for the reflection coefficient when compared with a closed-form solution. When applying the hybrid moment method procedures to a 3-D numerical test case with volume pulse-basis functions, good prediction of the scan blindness (E-plane scanning) and reflection coefficient is obtained. Finally, several waveguide simulator experiments were performed to validate the 3-D hybrid moment-method code. Very good agreement is observed between theory and measurements for several different array geometries.

II. Theory

Conventional moment-method and other full-wave solutions that employ dielectric substrate Green's functions are generally limited to geometries without transverse material inhomogeneities [2]. When inhomogeneities are present, only multilayer dielectric substrates have closed-form Green's functions [19], [20]. Newman and Tulyathan [21] successfully employed a moment method to solve the problem of an antenna in the presence of dielectric inhomogeneity by using volume pulse-basis functions to expand the polarization currents and good results for input impedance were obtained.

This paper extends the hybrid moment-method technique to solve the problem of an infinite periodic printed antenna array on a grounded homogeneous dielectric substrate with dielectric inhomogeneities, as shown in Fig. 2. This solution is general enough to treat each of the geometries shown in Fig. 1, as the conducting antenna element may be placed on the dielectric substrate on top of the dielectric block or below the dielectric block. Since we are implementing the hybrid moment method for periodic problems, the major tasks include: 1) deriving the necessary Green's functions for the homogeneous dielectric substrate; 2) choosing basis functions to expand the unknown equivalent surface and polarization current densities; 3) employing Galerkin's procedure; 4) solving the resulting matrix equation to obtain the current amplitudes; and 5) computing input impedance and reflection coefficient.

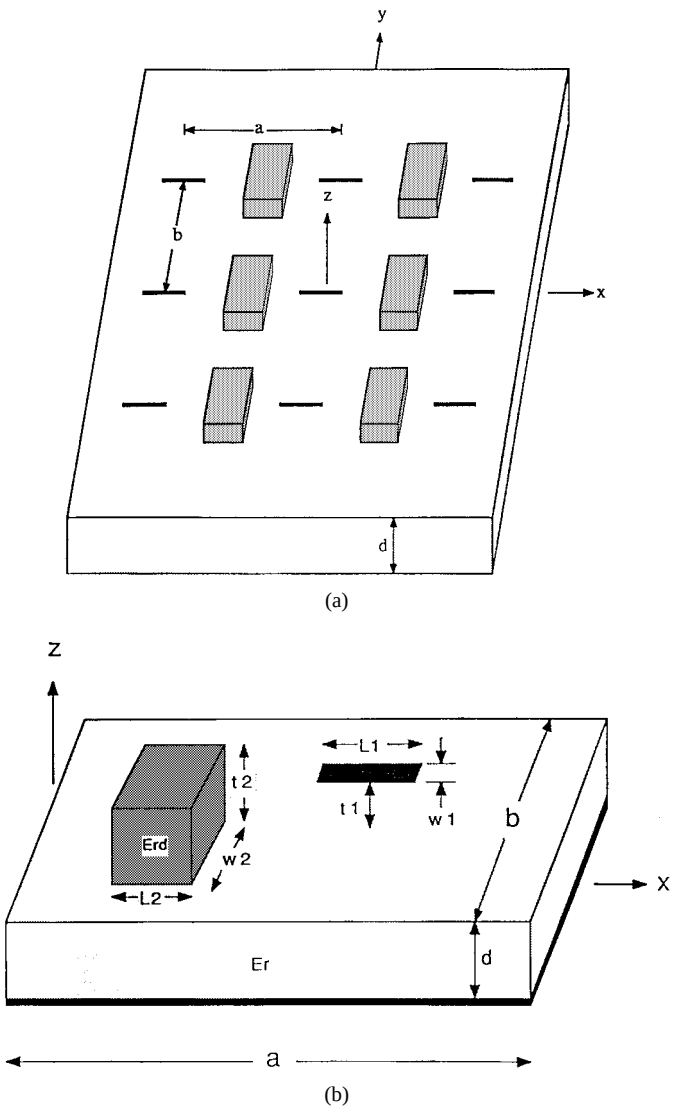

Fig. 2. (a) Infinite periodic printed dipole array on a homogeneous substrate with inhomogeneities. (b) Its unit cell configuration.

A. Dyadic Green's Function Formulations

Pozar and Schaubert [2] showed that the Poisson sum formula can be used to obtain the Green's function for an infinite array. In this work, the antenna and dielectric inhomogeneity are positioned on or above a grounded homogeneous dielectric slab, thus, the infinitesimal source current element must be positioned above the substrate $(z_0 > d)$ (detailed derivation is presented in [22]). In dyadic form, the Green's function for field and source points above the substrate can be expressed as

$$\overline{E}(x, y, z \mid x_0, y_0, z_0) = \hat{i}\hat{j}E_{ij}(x, y, z \mid x_0, y_0, z_0) \quad (1)$$

where $i, j = x, y,$ or z

$$E_{ij}(x, y, z \mid x_0, y_0, z_0) = \frac{1}{ab}\sum_{p=-\infty}^{\infty}\sum_{q=-\infty}^{\infty} G_{ij}(k_x, k_y, z \mid z_0) \cdot e^{-jk_x(x-x_0)}e^{-jk_y(y-y_0)}$$

$i = x$ or y or z, and $j = x$ or y or z.

The Green's function components G_{ij} are simple extensions to those given in [2] and [25] for

$z = z_0 = d$;
$k_x = k_0 u + \frac{2\pi p}{a}$;
$k_y = k_0 v + \frac{2\pi q}{b}$;
$u = \sin\theta\cos\phi$;
$v = \sin\theta\sin\phi$;
a is the unit cell dimension in the x direction, b is the unit cell dimension in the y direction; θ and ϕ are the scan angles, and p and q are integers representing discrete Floquet modes.

B. Integral Equation Derivation

Once the Green's functions are derived, the next task is to set up integral equations subject to required boundary conditions. Consider a unit cell of the infinite periodic printed array antenna with dielectric inhomogeneity, as shown in Fig. 2 (notice that the dipole is not necessarily on the substrate, but can be moved to any desired position t_1 above the substrate). Assume the surface current density induced on the conductor is $\vec{J}_s^w$ and that the volume polarization current density induced in the dielectric inhomogeneity is $\vec{J}_v^p$. Let

$\vec{E}^i$ be the incident field
$\vec{E}^w$ be the field due to $\vec{J}_s^w$ and
$\vec{E}^p$ be the field due to $\vec{J}_v^p$.

Then the tangential electric field must vanish on the conductor and the relationship between the total electric field and the volume polarization current density (from the volume equivalence theorem) can be used to create two integral equations. Since the tangential electric field must vanish on the conductor, we have

$$\vec{E}^{\rm tot}_{\rm tan} = (\vec{E}^i + \vec{E}^w + \vec{E}^p)_{\rm tan} = 0.$$

The above equation can be rewritten using the Green's function as

$$\vec{E}^i_{\rm tan} = -\vec{E}^w_{\rm tan} - \vec{E}^p_{\rm tan} = -\left(\int\int_{S_w} \overline{\overline{E}}\cdot\vec{J}_s^w\, ds_0\right)_{\rm tan} - \left(\int\int\int_{V_d} \overline{\overline{E}}\cdot\vec{J}_v^p\, dv_0\right)_{\rm tan}. \quad (2)$$

From the volume equivalence theorem [23], the induced volume polarization current density in the dielectric inhomogeneity is

$$\vec{J}_v^p = j\omega(\epsilon_d - \epsilon_0)\vec{E}^{\rm tot}.$$

Rearranging the above equation gives

$$\vec{E}^{\rm tot} = \frac{\vec{J}_v^p}{j\omega(\epsilon_d - \epsilon_0)} = \vec{E}^w + \vec{E}^p.$$

This can be expressed using the Green's function as

$$0 = -\int\int_{S_w} \overline{\overline{E}}\cdot\vec{J}_s^w\, ds_0 - \int\int\int_{V_d} \overline{\overline{E}}\cdot\vec{J}_v^p dv_0 + \frac{\vec{J}_v^p}{j\omega(\epsilon_d - \epsilon_0)}. \quad (3)$$

Equations (2) and (3) are the integral equations for the problem of an infinite periodic printed array antenna with the presence of a dielectric inhomogeneity.

C. Current Density Expansion and Reaction Impedance Generation

To carry out the moment-method solution, we need to choose basis functions to expand two unknown equivalent current densities $\vec{J}_s^w$ and $\vec{J}_v^p$. We use piecewise sinusoidal (PWS) modes for the conductor current and pulse functions to expand $\vec{J}_v^p$

$$\vec{J}_s^w = \hat{x}\sum_{n=1}^{N_w} I_n^w J_n^w \text{ and } \vec{J}_v^p = \hat{x}\sum_{n=N_w+1}^{N_w+N_v} I_{nx}^v J_n^p + \hat{y}\sum_{n=N_w+N_v+1}^{N_w+2N_v} I_{ny}^v J_n^p + \hat{z}\sum_{n=N_w+2N_v+1}^{N_w+3N_v} I_{nz}^v J_n^p$$

where

I_n^w, I_{nx}^v, I_{ny}^v, and I_{nz}^v are the unknown expansion coefficients and $J_n^w = \dfrac{\sin[k_e(h-|x-x_i|)]}{W\sin(k_e h)}$ for $|x-x_i| < h$ and $|y| < \dfrac{w}{2}$

is a piecewise-sinusoidal expansion mode with terminals at x_i, a half-length h, and $k_e = k_0\sqrt{\frac{\epsilon_r+1}{2}}$ (assuming a uniform distribution representing the current variation across the width w of the dipole)

$$J_n^p = \begin{cases} 1, & \text{for } x(n) \le x \le x(n+1),\ y(n) \le y \le y(n+1) \text{ and } z(n) \le z \le z(n+1) \\ 0, & \text{otherwise} \end{cases}$$

is a pulse-mode basis function for the dielectric inhomogeneity (the dielectric inhomogeneity is divided into small rectangular volumes, as shown in Fig. 3). N_w is the number of PWS modes on the conductor and N_v is the number of rectangular volumes in the dielectric inhomogeneity. The $x(n)$, $y(n)$, and $z(n)$ are the lowest corner coordinates of the nth parallelepiped as defined in Fig. 3.

The unknown current expansion coefficients I_n^w, I_{nx}^v, I_{ny}^v, and I_{nz}^v can be determined through Galerkin's procedure. First, we test (2) with $\vec{J}_m^w$ to obtain

$$\sum_{n=1}^{N_w} I_n^w Z_{mn}^{w-w} + \sum_{n=N_w+1}^{N_w+N_v} I_{nx}^v Z_{mnxx}^{w-v} + \sum_{n=N_w+N_v+1}^{N_w+2N_v} I_{ny}^v Z_{mnxy}^{w-v} + \sum_{n=N_w+2N_v+1}^{N_w+3N_v} I_{nz}^v Z_{mnxz}^{w-v} = V_m \quad (4)$$

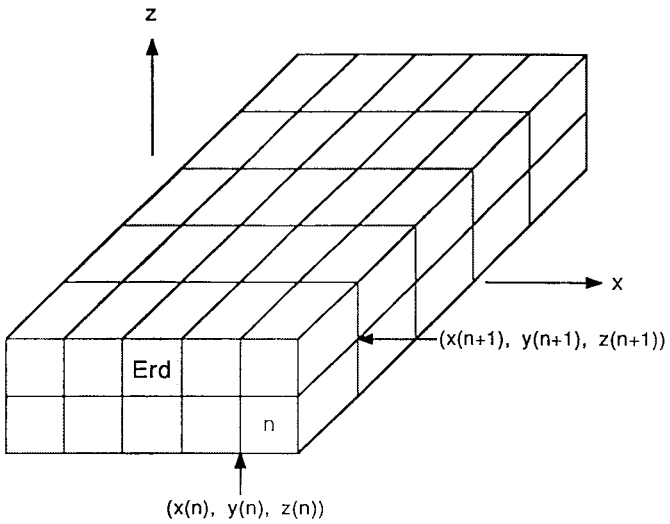

Fig. 3. Discretization of the dielectric inhomogeneity.

on the conductor $m = 1, 2, \cdots, N_w$, where

$$Z^{w-w}_{mn} = -\int\int_{S_{wm}} \int\int_{S_{wn}} G_{xx} J^w_m J^w_n \, dS_{on} \, dS_m$$

$$Z^{w-v}_{mnxi} = -\int\int_{S_{wm}} \int\int\int_{V_{dn}} G_{xi} J^w_m J^p_{ni} \, dV_{on} \, dS_m, \quad i = x \text{ or } y \text{ or } z.$$

Next, we test (3) with $\vec{J}^p_m$

$$\sum_{n=1}^{N_w} I^w_n Z^{v-w}_{mnxx} + \sum_{n=N_w+1}^{N_w+N_v} I^v_{nx} Z^{v-v}_{mnxx} + \sum_{n=N_w+N_v+1}^{N_w+2N_v} I^v_{ny} Z^{v-v}_{mnxy} + \sum_{n=N_w+2N_v+1}^{N} I^v_{nz} Z^{v-v}_{mnxz} - \frac{\eta_0}{k_0} \frac{j\Delta^3}{\epsilon_{rd}-1} \sum_{n=N_w+1}^{N_w+N_v} I^v_{nx} \delta(m-n) = 0 \quad (5)$$

in the dielectric inhomogeneity $m = N_w + 1, \cdots, N_w + N_v$, where

$$Z^{v-w}_{mnxx} = -\int\int\int_{V_{dm}} \int\int_{S_{wn}} G_{xx} J^p_{mx} J^w_n \, dS_{on} \, dV_m$$

$$Z^{v-v}_{mnxi} = -\int\int\int_{V_{dm}} \int\int\int_{V_{dn}} G_{xi} J^p_{mx} J^p_{ni} \, dV_{on} \, dV_m, \quad i = x \text{ or } y \text{ or } z$$

$$\delta(m-n) = \begin{cases} 1, & m = n \\ 0, & \text{otherwise} \end{cases}$$

and $\Delta = x(n+1) - x(n) = y(n+1) - y(n) = z(n+1) - z(n)$ is the spatial discretization step

$$\sum_{n=1}^{N_w} I^w_n Z^{v-w}_{mnyx} + \sum_{n=N_w+1}^{N_w+N_v} I^v_{nx} Z^{v-v}_{mnyx} + \sum_{n=N_w+N_v+1}^{N_w+2N_v} I^v_{ny} Z^{v-v}_{mnyy} + \sum_{n=N_w+2N_v+1}^{N} I^v_{nz} Z^{v-v}_{mnyz} - \frac{\eta_0}{k_0} \frac{j\Delta^3}{\epsilon_{rd}-1} \sum_{n=N_w+N_v+1}^{N_w+2N_v} I^v_{ny} \delta(m-n) = 0 \quad (6)$$

in the dielectric inhomogeneity $m = N_w + N_v + 1, \cdots, N_w + 2N_v$, where

$$Z^{v-w}_{mnyx} = -\int\int\int_{V_{dm}} \int\int_{S_{wn}} G_{yx} J^p_{\text{my}} J^w_n \, dS_{\text{on}} \, dV_m$$

$$Z^{v-v}_{mnyi} = -\int\int\int_{V_{dm}} \int\int\int_{V_{dn}} G_{yi} J^p_{my} J^p_{ni} \, dV_{\text{on}} \, dV_m, \quad i = x \text{ or } y \text{ or } z.$$

$$\sum_{n=1}^{N_w} I^w_n Z^{v-w}_{mnzx} + \sum_{n=N_w+1}^{N_w+N_v} I^v_{nx} Z^{v-v}_{mnzx} + \sum_{n=N_w+N_v+1}^{N_w+2N_v} I^v_{ny} Z^{v-v}_{mnzy} + \sum_{n=N_w+2N_v+1}^{N} I^v_{nz} Z^{v-v}_{mnzz} - \frac{\eta_0}{k_0} \frac{j\Delta^3}{\epsilon_{rd}-1} \sum_{n=N_w+2N_v+1}^{N} I^v_{nz} \delta(m-n) = 0 \quad (7)$$

in the dielectric inhomogeneity $m = N_w + 2N_v + 1, \cdots, N$, where

$$Z^{v-w}_{mnzx} = -\int\int\int_{V_{dm}} \int\int_{S_{wn}} G_{zx} J^p_{mz} J^w_n \, dS_{\text{on}} \, dV_m$$

$$Z^{v-v}_{mnzi} = -\int\int\int_{V_{dm}} \int\int\int_{V_{dn}} G_{zi} J^p_{mz} J^p_{ni} \, dV_{\text{on}} \, dV_m, \quad i = x \text{ or } y \text{ or } z.$$

When the volume polarization current density J^p_v is expanded by the pulse-mode basis functions, (4)–(7) can be written in more detail as

$$-\sum_{n=1}^{N_w} I^w_n \left\{ \frac{1}{ab} \sum_p \sum_q G^{ww}_{xx} F^*_m F_n \right\} - \sum_{n=N_w+1}^{N_w+N_v} I^v_{nx} \left\{ \frac{1}{ab} \sum_p \sum_q G^{wv}_{xx} F^*_m Q_n \right\} - \sum_{n=N_w+N_v+1}^{N_w+2N_v} I^v_{ny} \left\{ \frac{1}{ab} \sum_p \sum_q G^{wv}_{xy} F^*_m Q_n \right\} - \sum_{n=N_w+2N_v+1}^{N} I^v_{nz} \left\{ \frac{1}{ab} \sum_p \sum_q G^{ww}_{xz} F^*_m Q_n \right\} = V_m \quad (8)$$

on the conductor $m = 1, 2, \cdots, N_w$, where

$$V_m = \begin{cases} 1, & m = \frac{N_w+1}{2} \\ 0, & \text{otherwise.} \end{cases}$$

$$- \sum_{n=1}^{N_w} I_n^w \left\{ \frac{1}{ab} \sum_p \sum_q G_{xx}^{vw} Q_m^* F_n \right\}$$
$$- \sum_{n=N_w+1}^{N_w+N_v} I_{nx}^v \left\{ \frac{1}{ab} \sum_p \sum_q G_{xx}^{vv} Q_m^* Q_n \right\}$$
$$- \sum_{n=N_w+N_v+1}^{N_w+2N_v} I_{ny}^v \left\{ \frac{1}{ab} \sum_p \sum_q G_{xy}^{vv} Q_m^* Q_n \right\}$$
$$- \sum_{n=N_w+2N_v+1}^{N} I_{nz}^v \left\{ \frac{1}{ab} \sum_p \sum_q G_{xz}^{vv} Q_m^* Q_n \right\}$$
$$- \frac{\eta_0}{k_0} \frac{j\Delta^3}{\epsilon_{rd} - 1} \sum_{n=N_w+1}^{N_w+N_v} I_{nx}^v \delta(m-n) = 0 \tag{9}$$

in the dielectric inhomogeneity $m = N_w + 1, \cdots, N_w + N_v$

$$- \sum_{n=1}^{N_w} I_n^w \left\{ \frac{1}{ab} \sum_p \sum_q G_{yx}^{vw} Q_m^* F_n \right\}$$
$$- \sum_{n=N_w+1}^{N_w+N_v} I_{nx}^v \left\{ \frac{1}{ab} \sum_p \sum_q G_{yx}^{vv} Q_m^* Q_n \right\}$$
$$- \sum_{n=N_w+N_v+1}^{N_w+2N_v} I_{ny}^v \left\{ \frac{1}{ab} \sum_p \sum_q G_{yy}^{vv} Q_m^* Q_n \right\}$$
$$- \sum_{n=N_w+2N_v+1}^{N} I_{nz}^v \left\{ \frac{1}{ab} \sum_p \sum_q G_{yz}^{vv} Q_m^* Q_n \right\}$$
$$- \frac{\eta_0}{k_0} \frac{j\Delta^3}{\epsilon_{rd} - 1} \sum_{n=N_w+N_v+1}^{N_w+2N_v} I_{ny}^v \delta(m-n) = 0 \tag{10}$$

in the dielectric inhomogeneity $m = N_w + N_v + 1, \cdots, N_w + 2N_v$

$$- \sum_{n=1}^{N_w} I_n^w \left\{ \frac{1}{ab} \sum_p \sum_q G_{zx}^{vw} Q_m^* F_n \right\}$$
$$- \sum_{n=N_w+1}^{N_w+N_v} I_{nx}^v \left\{ \frac{1}{ab} \sum_p \sum_q G_{zx}^{vv} Q_m^* Q_n \right\}$$
$$- \sum_{n=N_w+N_v+1}^{N_w+2N_v} I_{ny}^v \left\{ \frac{1}{ab} \sum_p \sum_q G_{zy}^{vv} Q_m^* Q_n \right\}$$
$$- \sum_{n=N_w+2N_v+1}^{N} I_{nz}^v \left\{ \frac{1}{ab} \sum_p \sum_q G_{zz}^{vv} Q_m^* Q_n \right\}$$
$$- \frac{\eta_0}{k_0} \frac{j\Delta^3}{\epsilon_{rd} - 1} \sum_{n=N_w+2N_v+1}^{N} I_{nz}^v \delta(m-n) = 0 \tag{11}$$

in the dielectric inhomogeneity $m = N_w + 2N_v + 1, \cdots, N$. Detail expression of those related functions can be found in [22].

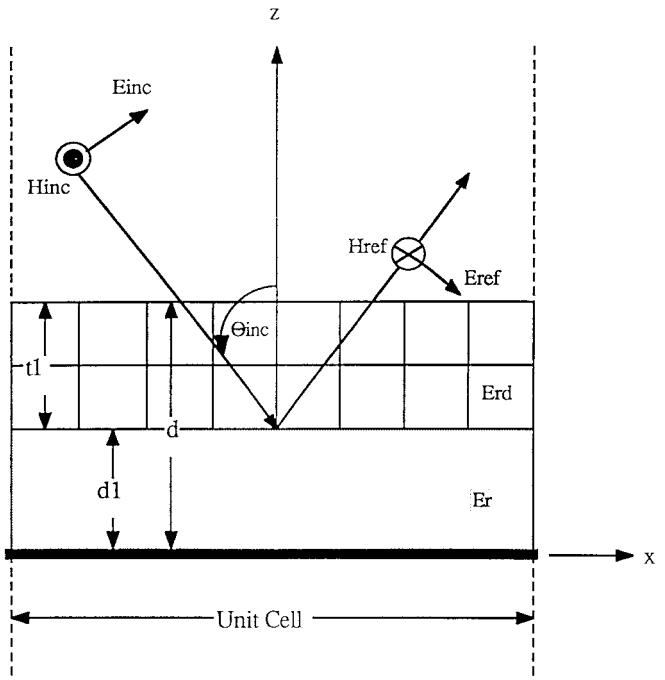

Fig. 4. Two-dimensional plane wave scattering from a grounded dielectric slab.

Equations (4)–(7) form $N = N_w + 3N_v$ linear equations with N unknown current expansion coefficients, which can be shown in matrix representation as

$$\begin{bmatrix} [Z^{w-w}] & [Z^{w-v}] \\ [Z^{v-w}] & [Z^{v-v}] \end{bmatrix} \begin{bmatrix} [I^w] \\ [I^v] \end{bmatrix} = \begin{bmatrix} [V^w] \\ [O] \end{bmatrix}. \tag{12}$$

The expansion coefficients I^w and I^v can be obtained by solving the matrix equation (12). The input impedance at a center-fed dipole element in the array is defined as

$$Z_{\text{in}}(\theta, \phi) = \frac{V_k}{I_k}, \qquad \text{where } k = \frac{N_w + 1}{2}. \tag{13}$$

Then the active reflection coefficient [2] can be calculated as

$$R(\theta, \phi) = \frac{Z_{\text{in}}(\theta, \phi) - Z_{\text{in}}(0, 0)}{Z_{\text{in}}(\theta, \phi) + Z_{\text{in}}^*(0, 0)}. \tag{14}$$

This completes the hybrid moment-method formulation for an infinite-periodic printed-array antenna with a dielectric inhomogeneity. Since the reaction impedance formulation for the dielectric inhomogeneity itself is quite complicated, it is useful to validate this part separately. Two-dimensional plane wave scattering from a grounded dielectric slab is sufficient to serve this purpose, as will be explained in the following section.

D. 2-D Plane Wave Scattering from a Grounded Dielectric Slab

Consider a parallel polarized uniform plane wave incident on a grounded dielectric slab, as shown in Fig. 4. The incident and reflected plane waves can be expressed as

$$\vec{E}^i(x, z) = [\hat{x} \cos(\theta_i) + \hat{z} \sin(\theta_i)] \cdot e^{-jk_0[x \sin(\theta_i) - (z - d_1)\cos(\theta_i)]} \tag{15}$$

$$\vec{E}^r(x,\,z) = \Gamma_{\rm par}[\hat{x}\cos(\theta_{\rm i}) - \hat{\rm z}\sin(\theta_{\rm i})] \cdot e^{-jk_0[x\sin(\theta_{\rm i})+({\rm z}-{\rm d}_1)\cos(\theta_{\rm i})]} \tag{16}$$

where $\Gamma_{\rm par}$ is the parallel polarization reflection coefficient at $z = d_1$, which is known in closed form [26], θ_i is the incidence angle, and θ_t is the transmission angle.

In order to incorporate the reaction impedance formulation for a dielectric inhomogeneity into the problem, we divide the original grounded dielectric slab of thickness d into a thinner grounded homogeneous dielectric slab of thickness d_1 and a dielectric layer with thickness $t_1 = d - d_1$ to be modeled using volume polarization currents. Then we have two cases for comparison. One is the canonical problem of the reflected field of a grounded dielectric slab with thickness d with no polarization currents. The other is the reflected field of a homogeneous grounded dielectric slab of thickness d_1, plus the scattered field due to the discretized volumetric modeling of the remaining layer of thickness t_1. Obviously, these two cases should be equivalent.

The scattered field and current density inside the dielectric layer of thickness t_1 in the presence of a grounded dielectric slab of thickness d_1 can be written as e14

$$\vec{E}^s = \vec{E}^{\rm total} - \vec{E}^i - \vec{E}^r = \int\int_{S_d} \overline{\overline{E}} \cdot \vec{J}^p\, dS_0 \quad \text{and } \vec{J}^p = j\omega\epsilon_0(\epsilon_{rd}-1)\vec{E}^{\rm total}.$$

Rearranging the above equations gives an integral equation as

$$-\int\int_{S_d} \overline{\overline{E}} \cdot \vec{J}^p\, dS_0 + \frac{\vec{J}^p}{j\omega\epsilon_0(\epsilon_{rd}-1)} = \vec{E}^i + \vec{E}^r. \tag{17}$$

Now, we let

$$\vec{J}^p = \hat{x}\sum_{n=1}^{N_v} I^v_{nx} J^p_n + \hat{z}\sum_{n=N_v+1}^{2N_v} I^v_{nz} J^p_n \text{ where}$$

$$J^p_n = \begin{cases} 1, & \text{for } x(n) \le x \le x(n+1) \text{ and} \\ & z(n) \le z \le z(n+1) \\ 0, & \text{otherwise} \end{cases}$$

is a pulse-mode basis function for the dielectric layer.

Using the standard Galerkin's procedure, we obtain the following equations:

$$-\sum_{n=1}^{N_v} I^v_{nx}\left\{\frac{1}{a}\sum_p G^{vv}_{xx} Q^*_m Q_n\right\} - \sum_{n=N_v+1}^{N} I^v_{nz}\left\{\frac{1}{a}\sum_p G^{vv}_{xz} Q^*_m Q_n\right\} - \frac{\eta_0}{k_0}\frac{j\Delta_x\Delta_z}{\epsilon_{rd}-1}\sum_{n=1}^{N_v} I^v_{nx}\delta(m-n) = V^1_m \tag{18}$$

in the dielectric layer $m = 1, \cdots, N_v$ and

$$-\sum_{n=1}^{N_v} I^v_{nx}\left\{\frac{1}{a}\sum_p G^{vv}_{zx} Q^*_m Q_n\right\} - \sum_{n=N_v+1}^{N} I^v_{nz}\left\{\frac{1}{a}\sum_p G^{vv}_{zz} Q^*_m Q_n\right\} - \frac{\eta_0}{k_0}\frac{j\Delta_x\Delta_z}{\epsilon_{rd}-1}\sum_{n=N_v+1}^{N} I^v_{nz}\delta(m-n) = V^2_m \tag{19}$$

in the dielectric layer $m = N_v + 1, \cdots, N$. Definition of all the related functions can be found in [22].

Once the unknown current expansion coefficients are found through the standard matrix formulation of the moment method, the scattered field due to the dielectric layer can be easily obtained. The reflection coefficient of a plane wave incident on a grounded dielectric slab of thickness d is equal to the reflected field of the grounded dielectric slab of thickness d_1, plus the scattered field of the discretized dielectric layer of thickness t_1 divided by the incident field amplitude

$$\Gamma_{\rm par} = \frac{E^r_x(z=d) + E^s_x(x = t_1\tan(\theta_{\rm i}),\, {\rm z} = {\rm d})}{{\rm E}^{\rm i}_{\rm x}({\rm z} = {\rm d})} \tag{20}$$

where

$$E^i_x(z=d) = \cos(\theta_{\rm i}){\rm e}^{-{\rm jk}_0\sin(\theta_{\rm i})[{\rm t}_1\tan(\theta_{\rm i})]}$$

$$E^r_x(z=d) = \Gamma_{\rm par}(z=d_1)\cos(\theta_{\rm i}) \cdot e^{-jk_0\sin(\theta_{\rm i})[{\rm t}_1\tan(\theta_{\rm i})]}e^{-jk_0\cos(\theta_i)2t_1}.$$

Since we use pulse-mode basis functions to model the dielectric layer, fictitious surface charges will be introduced on the interface of adjacent discretization cells, which may cause the solution to converge slower. To see the effect of these fictitious charges, we selected discretization steps of $0.1\lambda_0$, $0.05\lambda_0$, and $0.025\lambda_0$ to verify the convergent speed. Both magnitude and phase of the reflection coefficient were compared with the closed-form solution. The magnitude always maintains at least six significant digit accuracy and the phase error improves from 1 to 0.1%. These results seem to suggest that as long as the discretization step is smaller than $0.025\lambda_0$, those fictitious surface charges will not have a significant effect on the moment-method solution as compared with the closed-form solution.

The 2-D scattering formulation provides a good validation for the 3-D scattering formulation, because all the key integrations in the 3-D formulation are in the z direction, while in the 2-D formulation, the same functions are used. The differences between the 2-D and 3-D formulations are simply: 1) two summations of k_x and k_y are replaced with only one k_x summation and 2) k_y drops to zero for all the Green's functions in the 2-D case. This simpler problem thus offers a necessary but not completely sufficient analytical check on the solution. Further validation of the 3-D results are provided by comparison with measured data from waveguide simulator experiments, as discussed in the following section.

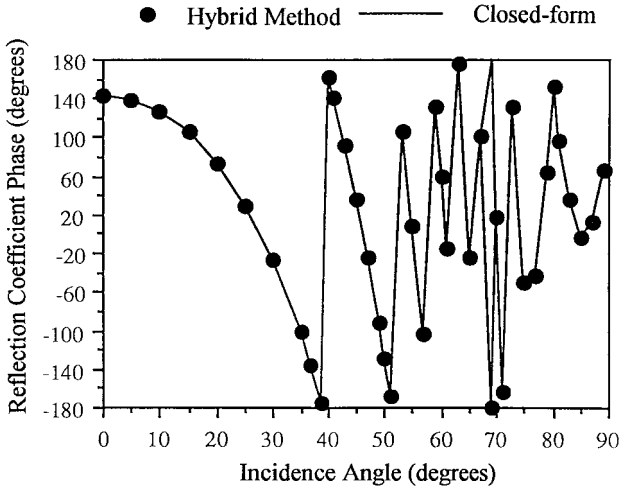

Fig. 5. Phase of the reflection coefficient of a 2-D grounded dielectric slab with $d_1 = 0.1\lambda_0$ and $t_1 = 0.1\lambda_0$.

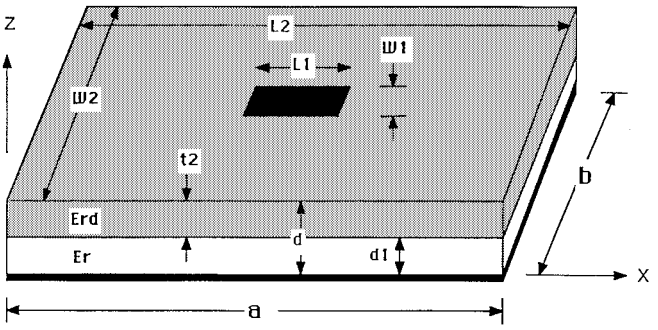

Fig. 6. Unit cell of an infinite array of printed dipoles on a dielectric substrate, modeled using the hybrid MoM solution for comparison with homogeneous substrate solution.

III. Validations and Results

To check the self- and mutual-reaction impedances for the volume polarization currents, the example of 2-D plane wave scattering from a grounded dielectric slab is used. Since all the media are assumed lossless, the magnitude of the reflection coefficient should be unity. Fig. 5 shows the phase of the reflection coefficient where $d_1 = 0.1\lambda_0$, $t_1 = 0.1\lambda_0$, $d = d_1 + t_1$, and $\epsilon_r = 2.55$. An excellent agreement (the error is within 0.3 degree) is observed when compared with the closed-form solution for a spatial discretization smaller than $0.025\,\lambda_0$. The hybrid moment-method solution takes about 7 s per data point on a DEC3000 AXP workstation.

Next, a 3-D test case of an infinite printed dipole array [2] was used to verify the hybrid MoM code, as shown in Fig. 6. The bottom substrate layer of thickness d_1 is handled exactly through the Green's function, while the top layer of thickness t_2 is discretized using volume polarization current basis functions. The array input impedance (or reflection coefficient) of an element in the infinite periodic printed dipole array with a homogeneous substrate of thickness d should be equal to the impedance (or reflection coefficient) of the array shown in Fig. 6, which consists of a homogeneous dielectric slab of thickness d_1 and a layer of thickness t_2 modeled with volume polarization currents. The parameters for this test

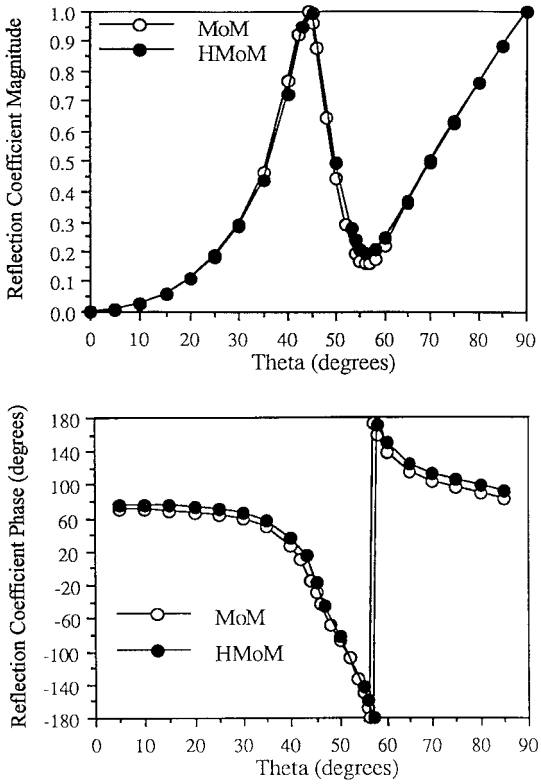

Fig. 7. Comparison of the magnitude and phase of the reflection coefficient from the MoM and the hybrid MoM solutions for an infinite array of printed dipoles on a homogeneous substrate.

case were chosen as follows: $d = 0.19\lambda_0$, $d_1 = 0.165\lambda_0$, $a = 0.5\lambda_0$, $b = 0.1\lambda_0$, $L_1 = 0.39\lambda_0$, $W_1 = 0.002\lambda_0$, $L_2 = 0.5\lambda_0$, $W_2 = 0.1\lambda_0$, $t_2 = 0.025\lambda_0$, $\epsilon_r = 2.55$, and $\epsilon_{rd} = 2.55$. With E-plane scanning ($\phi = 0°$) and a spatial discretization of $\Delta = 0.0125\lambda_0$, the magnitude and phase of the reflection coefficient of the hybrid MoM solution show good agreement with that of the MoM solution described in [2], as shown in Fig. 7.

The first waveguide simulator was fabricated with a thick substrate to produce a pronounced scan blindness. The waveguide was standard brass H-band (4–6 GHz) guide, with inner dimensions of 4.755 cm $\times$ 2.215 cm. Two printed monopoles (fed with a power divider) of length 1.85 cm and width 0.19 cm were laid on a plexiglass substrate of thickness $d = 1.86$ cm, permittivity $\epsilon_r = 2.60$, and loss tangent of 0.0057 [24]. The element spacings were $a = 4.43$ cm and $b = 2.38$ cm. A de-embedding technique [22] was used to remove the loss and phase shift effects of the two-way power divider from the measured data. Fig. 8 shows good agreement for the magnitude and phase of the reflection coefficient from the hybrid MoM solution and the waveguide simulator experimental result. Notice that the scan blindness occurs at 4.99 GHz with a measured reflection coefficient magnitude of 0.89. This nonunity value is the result of copper and dielectric loss in the simulator.

One purpose of this work was to obtain extra degrees of freedom for an infinite periodic array by introduction of a dielectric inhomogeneity to allow improved bandwidth without the usual concomitant scan blindness that occurs with a thick

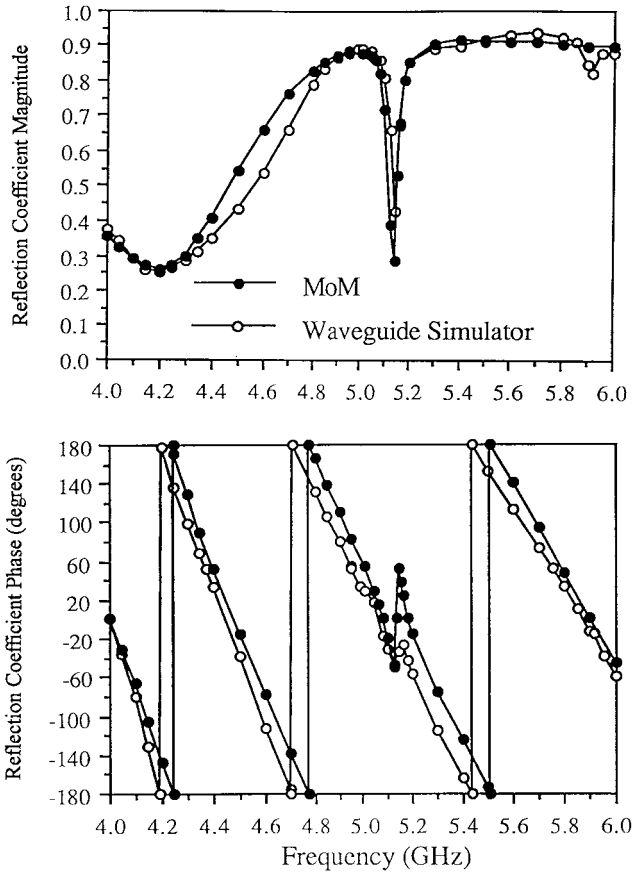

Fig. 8. Comparison of the magnitude and phase of the reflection coefficient calculated from the hybrid MoM solution, and measured in a waveguide simulator for an infinite dipole array on a uniform dielectric substrate [Fig. 1(a)].

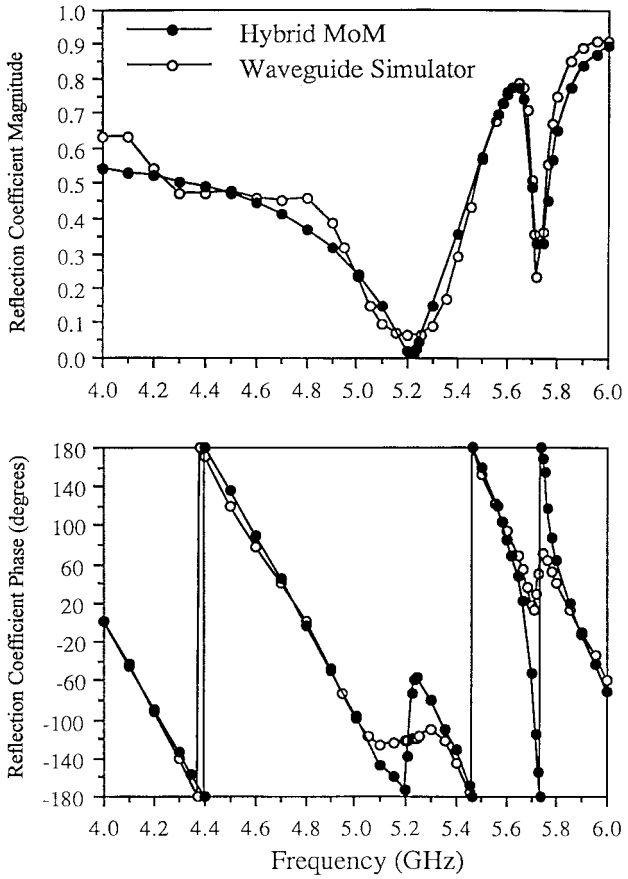

Fig. 9. Comparison of the magnitude and phase of the reflection coefficient calculated from the hybrid MoM solution and measured in a waveguide simulator for an infinite dipole array on an inhomogeneous dielectric substrate of the type shown in Fig. 1(c).

substrate. After some numerical testing, the geometry shown in Fig. 1(b) did not achieve this objective due to the fact that it failed to reduce the surface wave coupling between dipoles. However, the geometries shown in Fig. 1(c) and (d) proved to be better candidates for this purpose. It is well known that a thick substrate for an infinite periodic printed dipole array improves bandwidth, but at the expense of a smaller available scan range due to the excitation of surface waves and the resulting scan blindness. If the height from the ground plane to the dipole is fixed at d as shown in Fig. 1(a), we can trim away part of the substrate to give the geometry shown in Fig. 1(c). By doing so, the effective substrate thickness is reduced away from the dipoles and the scan blindness effect can be alleviated significantly.

In order to show a pronounced change in the occurrence of scan blindness, the previous waveguide simulator was refabricated to use the inhomogeneous substrate geometry shown in Fig. 1(c). The same printed monopole of length 1.85 cm and width 0.19 cm was laid on a plexiglass support post of length $L_2 = 2$ cm, width $W_2 = 0.28$ cm, thickness $t_2 = 0.86$ cm, permittivity $\epsilon_r = 2.60$, and loss tangent 0.0057. The substrate was also plexiglass with thickness $d_1 = 1$ cm, permittivity $\epsilon_r = 2.60$, and loss tangent 0.0057. The element spacings were $a = 4.43$ cm and $b = 2.38$ cm. Fig. 9 shows a good agreement for the magnitude and phase of the reflection coefficient between the hybrid MoM solution and the waveguide simulator experimental result. Notice that the scan blindness moves from the previous frequency of 4.99 up to 5.64 GHz. Using the surface wave theory of scan blindness discussed in [2], the blindness angle of 39.2° at 4.99 GHz for the array of Fig. 8 corresponds to an effective surface wave propagation constant of $\beta_{sw}/k_0 = \lambda/b - \sin\theta_b = 1.889$. For the array of Fig. 9, however, the blindness angle of 33.9° at 5.64 GHz implies an effective surface wave propagation constant of $\beta_{sw}/k_0 = 1.676$. While both of these values are atypically large for purposes of illustration, the significant reduction of the surface wave propagation constant means that blindness for E plane scanning will occur further from broadside for the array of Fig. 9 due to the inhomogeneous dielectric.

The dielectric overlay has been suggested to increase the bandwidth of printed antennas [5], [6]. Also, with a small modification of the feeding structure, we can model a dielectric disk resonator antenna above the grounded dielectric substrate [7]. For these two applications, the structure shown in Fig. 1(d) is relevant. A third waveguide simulator was fabricated to validate the hybrid MoM solution for this geometry. Two printed monopoles of length 1.2 cm and width 0.2 cm were laid on a plexiglass substrate of thickness $d_1 = 1.05$ cm, permittivity $\epsilon_r = 2.60$, and loss tangent 0.0057. The dielectric overlay was also plexiglass, with length $L_2 = 1.7$ cm,

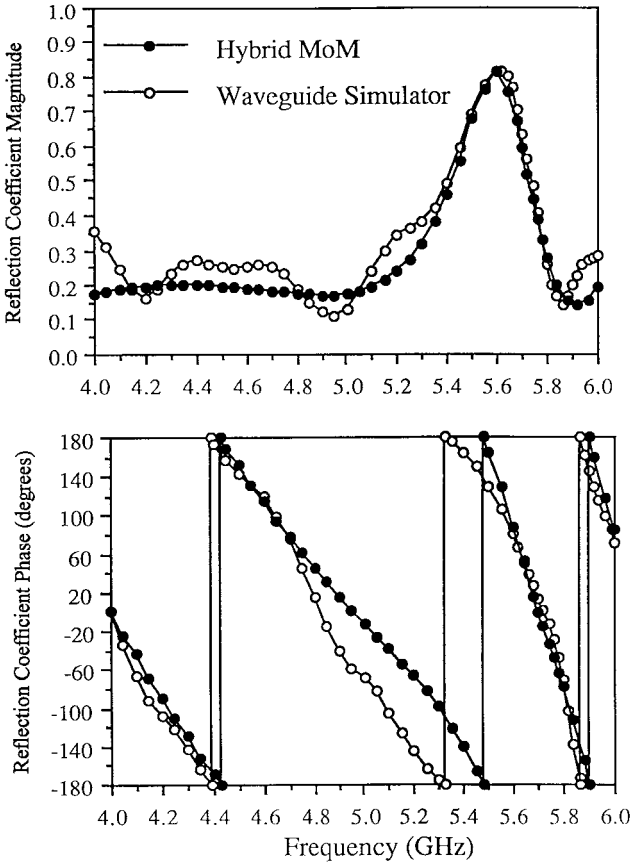

Fig. 10. Comparison of the magnitude and phase of the reflection coefficient calculated from the hybrid MoM solution and measured in a waveguide simulator for an infinite dipole array on an inhomogeneous dielectric substrate of the type shown in Fig. 1(d).

width $W_2 = 0.6$ cm, thickness $t_2 = 0.38$ cm, permittivity $\epsilon_r = 2.60$, and loss tangent 0.0057. The element spacings were $a = 4.43$ cm and $b = 2.38$ cm. In general, Fig. 10 shows a good agreement for the magnitude and phase of the reflection coefficient between the hybrid MoM solution and the waveguide simulator experimental result. Some of the difference between measured and calculated results is probably due to measurement and fabrication tolerance. The "rounding" of nulls and peaks in the calculated data is probably due to discretization error. For broadside radiation, Fig. 11 shows a noticeable bandwidth increase with the dielectric overlays, in contrast to the same array without the overlays. A simple explanation for this bandwidth enhancement is that the dielectric overlay is slightly larger than the dipole, so two relatively close resonant frequencies contribute to this bandwidth increase. Notice that the scan blindness occurs at 5.61 GHz, whereas the scan blindness occurs at 4.93 GHz when the homogeneous substrate thickness d is equal to 1.86 cm. This is another example of the significant shift in the scan blindness angle.

IV. Conclusion

The hybrid moment method has been developed and applied to infinite periodic antennas and scatterers having dielectric inhomogeneities and printed conductor radiating elements. The conducting element was modeled using PWS mode electric surface current basis functions and the dielectric inhomogeneity was modeled using pulse-mode equivalent volume current basis functions. Two coupled integral equations were derived and a Galerkin procedure was implemented.

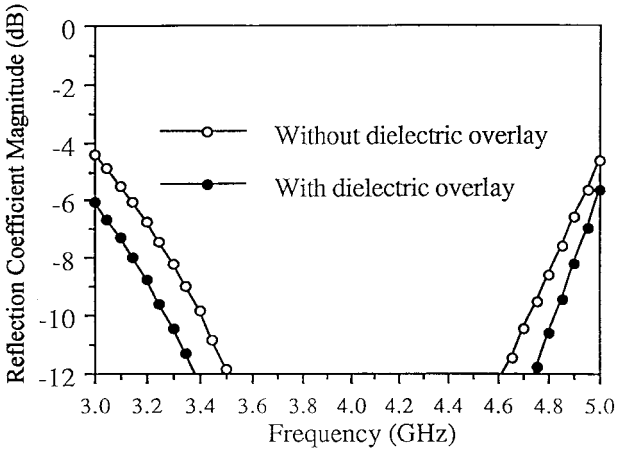

Fig. 11. Comparison of the frequency bandwidth for an infinite periodic printed dipole array with and without dielectric overlays.

Several numerical and experimental test cases were used to validate the hybrid MoM computer code. A numerical result for 2-D plane wave scattering from a grounded dielectric slab was used to validate the self- and mutual-reaction impedances of the dielectric inhomogeneity. Even though surface fictitious charges are introduced in the process of expanding the polarized current density in the dielectric layer, good agreement was observed when compared with the closed-form solution.

Waveguide simulators were built to validate the calculations from the hybrid moment method. By using dielectric supports or overlays, we are able to introduce a degree of freedom to resolve the usual tradeoff between frequency bandwidth and available scan range in printed phased arrays. Waveguide simulators were used for validation of several geometries, showing a significant shift in the scan blindness angle. A typical hybrid MoM solution requires about 40-min CPU time per data point when running on a DEC3000 AXP workstation.

References

[1] E. H. Newman, "An overview of the hybrid MM/Green's function method in electromagnetics," *Proc. IEEE*, vol. 76, pp. 270–282, Mar. 1988.

[2] D. M. Pozar and D. H. Schaubert, "Scan blindness in infinite phased arrays of printed dipoles," *IEEE Trans. Antennas Propagat.*, vol. AP-32, pp. 602–610, June 1984.

[3] M. Davidovitz, "Extension of the E-plane scanning range in large microstrip arrays by substrate modification," *IEEE Microwave Guided Wave Lett.*, vol. 2, pp. 492–494, Dec. 1992.

[4] J. R. Bayard, D. H. Schaubert, and M. E. Cooley, "E-plane scan performance of infinite arrays of dipoles printed on protruding dielectric substrate: coplanar feed line and E-plane metallic wave effects," *IEEE Trans. Antennas Propagat.*, vol. 41, pp. 837–841, June 1993.

[5] A. Henderson, J. R. James, and C. M. Hall, "Bandwidth extension techniques in printed conformal antennas," Military Microwaves, MM86, Brighton, U.K., June 1986.

[6] P. S. Hall, C. Wood, and C. Garrett, "Wide bandwidth microstrip antennas for circuit integration," *Electron. Lett.*, vol. 15, pp. 458–459, 1979.

[7] M. W. McAllister, S. A. Long, and G. L. Conway, "Rectangular dielectric resonator antenna," *Electron. Lett.*, vol. 19, pp. 218–219, 1983.

[8] A. A. Kishk, M. R. Zunoubi, and D. Kajfez, "A numerical study of a dielectric disk antenna above grounded dielectric substrate," *IEEE Trans. Antennas Propagat.*, vol. 41, pp. 813–821, June 1993.
[9] K. R. Umashankar and A. Taflove, "A novel method to analyze electromagnetic scattering of complex objects," *IEEE Trans. Electromagn. Compat.*, vol. EMC-24, pp. 397–405, Nov. 1982.
[10] C. Wu, K. Wu, Z. Bi, and J. Litva, "Accurate characterization of planar printed antennas using FDTD method," *IEEE Trans. Antennas Propagat.*, vol. 40, pp. 526–534, May 1992.
[11] J. Maloney, G. Smith, and W. Scott, "Accurate computation of the radiation from simple antennas using the FDTD method," *IEEE Trans. Antennas Propagat.*, vol. 38, pp. 1059–1068, July 1990.
[12] W. L. Ko and R. Mittra, "Implementation of Floquet boundary condition in FDTD for FSS analysis," in *IEEE AP-S Int. Symp. Dig.*, Ann Arbor, MI, June 1993, pp. 14–17.
[13] W. J. Tsay and D. M. Pozar, "Application of the FDTD technique to periodic problems in scattering and radiation," *IEEE Microwave Guided Wave Lett.*, vol. 3, pp. 250–252, Aug. 1993.
[14] J. Ren, O. P. Gandhi, L. R. Walker, J. Fraschilla, and C. R. Boerman, "Floquet-based FDTD analysis of two-dimensional phased array antennas," *IEEE Microwave Guided Wave Lett.*, vol. 4, pp. 109–111, Apr. 1994.
[15] P. Harms, R. Mittra, and W. L. Ko, "Implementation of the periodic boundary condition in the finite-difference time-domain algorithm for FSS structures," in *IEEE AP-S Int. Symp. Dig.*, Seattle, WA, June 1994, vol. 3, pp. 2144–2147.
[16] D. T. Prescott and N. V. Shuley, "A technique for analyzing frequency selective surfaces using the finite-difference time-domain method," in *IEEE AP-S Int. Symp. Dig.*, Seattle, WA, June 1994, vol. 3, pp. 2152–2155.
[17] J. Richmond, "On the edge mode in the theory of TM scattering by a strip or strip grating," *IEEE Trans. Antennas Propagat.*, vol. AP-28, pp. 883–887, Nov. 1980.
[18] T. K. Sarkar and E. Arvas, "An integral equation approach to the analysis of finite microstrip antennas: volume/surface formulation," *IEEE Trans. Antennas Propagat.*, vol. 38, pp. 305–312, Mar. 1990.
[19] T. Itoh, "Spectral domain immittance approach for dispersion characteristics of generalized printed transmission lines," *IEEE Trans. Microwave Theory Tech.*, vol. MTT-28, pp. 733–736, July 1980.
[20] N. K. Das and D. M. Pozar, "A generalized spectral-domain Green's function for multilayer dielectric substrates with application to multilayer transmission lines," *IEEE Trans. Microwave Theory Tech.*, vol. MTT-35, pp. 326–335, Mar. 1987.
[21] E. H. Newman and P. Tulyathan, "Wire antennas in the presence of a dielectric-ferrite inhomogeneity," *IEEE Trans. Antennas Propagat.*, vol. AP-26, pp. 587–593, July 1978.
[22] W. J. Tsay, "Radiation and scattering from periodic geometries in inhomogeneous media," Ph.D. dissertation, Univ. Massachusetts at Amherst, 1995.
[23] C. A. Balanis, *Advanced Engineering Electromagnetics.* New York: Wiley, 1989.
[24] D. M. Pozar, *Microwave Engineering.* Reading, MA: Addison-Wesley, 1990.
[25] J. T. Aberle and D. M. Pozar, "Analysis of infinite arrays of probe-fed rectangular microstrip patches using a rigorous feed model," *Proc. Inst. Elect. Eng.*, vol. 136, pt. H, no. 2, pp. 110–119, Apr. 1989.
[26] M. E. Cooley, "Analysis of infinite arrays of endfire slot antennas," Ph.D. dissertation, Univ. Massachusetts at Amherst, 1992.

Wen-Jiunn Tsay was born in Hsinchu, Taiwan, in 1960. He received the B.S. degree in electronic engineering from National Chiao Tung University, Hsinchu, Taiwan, in 1982, the M.S. degree from Arizona State University, Tempe, in 1991, and the Ph.D. degree from the University of Massachusetts at Amherst in 1995.

From 1982 to 1986, he served at the R.O.C. Army Headquarters and was the Deputy Commander of one electronic warfare company. From 1986 to 1988 he was with Microelectronics Technology Inc. as a Research and Development Engineer. Since 1995 he has been employed at Anritsu/Wiltron Company, Morgan Hill, CA.

David M. Pozar (S'74–M'80–SM'88–F'90), for a photograph and biography, see p. 1625 of the November 1997 issue of this TRANSACTIONS.